

# L-Threonine Transaldolase Activity Is Enabled by a Persistent Catalytic Intermediate

Prasanth Kumar,<sup>§</sup> Anthony Meza,<sup>§</sup> Jonathan M. Ellis, Grace A. Carlson, Craig A. Bingman, and Andrew R. Buller\*



Cite This: <https://dx.doi.org/10.1021/acscchembio.0c00753>



Read Online

ACCESS |



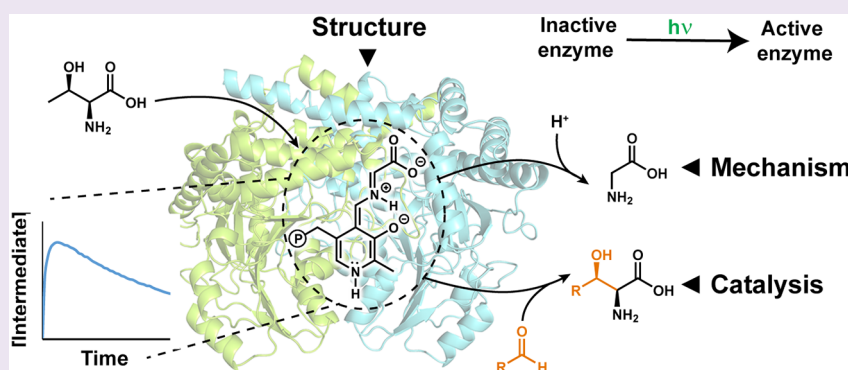
Metrics & More



Article Recommendations



Supporting Information



**ABSTRACT:** L-Threonine transaldolases (LTTAs) are a poorly characterized class of pyridoxal-5'-phosphate (PLP) dependent enzymes responsible for the biosynthesis of diverse  $\beta$ -hydroxy amino acids. Here, we study the catalytic mechanism of ObiH, an LTTA essential for biosynthesis of the  $\beta$ -lactone natural product obafluorin. Heterologously expressed ObiH purifies as a mixture of chemical states including a catalytically inactive form of the PLP cofactor. Photoexcitation of ObiH promotes the conversion of the inactive state of the enzyme to the active form. UV-vis spectroscopic analysis reveals that ObiH catalyzes the retro-aldol cleavage of L-threonine to form a remarkably persistent glycyl quinonoid intermediate, with a half-life of  $\sim 3$  h. Protonation of this intermediate is kinetically disfavored, enabling on-cycle reactivity with aldehydes to form  $\beta$ -hydroxy amino acids. We demonstrate the synthetic potential of ObiH via the single step synthesis of (2*S*,3*R*)- $\beta$ -hydroxyisoleucine. To further understand the structural features underpinning this desirable reactivity, we determined the crystal structure of ObiH bound to PLP as the Schiff's base at 1.66 Å resolution. This high-resolution model revealed a unique active site configuration wherein the evolutionarily conserved Asp that traditionally H-bonds to the cofactor is swapped for a neighboring Glu. Molecular dynamics simulations combined with mutagenesis studies indicate that a structural rearrangement is associated with L-threonine entry into the catalytic cycle. Together, these data explain the basis for the unique reactivity of LTTA enzymes and provide a foundation for future engineering and mechanistic analysis.

## INTRODUCTION

Nature often employs noncanonical amino acids that bear new and different functional groups to tune the properties of bioactive small molecules.<sup>1,2</sup> There are dozens of known modifications to proteogenic amino acids, including a wide variety that bear a hydroxyl group at the  $\beta$ -carbon. Such  $\beta$ -hydroxy amino acids are building blocks of complex natural products with a wide range of biological activities [*e.g.*, sphingofungin (antifungal),<sup>3</sup> salinosporamide (anticancer),<sup>4</sup> and cyclosporin (immunosuppressant)<sup>5</sup>] (Figure 1a).  $\beta$ -Hydroxy amino acids are also common synthetic precursors to  $\beta$ -lactams<sup>6</sup> and aziridine carboxylic acid derivatives<sup>7</sup> in synthetic chemistry and as precursors to chiral bisoxazoline ligands for metal catalysis.<sup>8</sup> The medicinal utility of these amino acids range from the treatment of Alzheimer's disease

(Droxidopa)<sup>9</sup> to the synthesis of antibiotic analogues (vancomycin and chloramphenicol).<sup>10</sup> These diverse applications underlie a broad interest in understanding  $\beta$ -hydroxy amino acid production and utilization in nature.

Mirroring the myriad bioactive molecules that harbor  $\beta$ -hydroxy amino acids, nature has evolved multiple biosynthetic routes to produce these useful compounds. Free amino acids can undergo stereospecific  $C\beta$  hydroxylation, as illustrated by

Received: September 20, 2020

Accepted: December 10, 2020



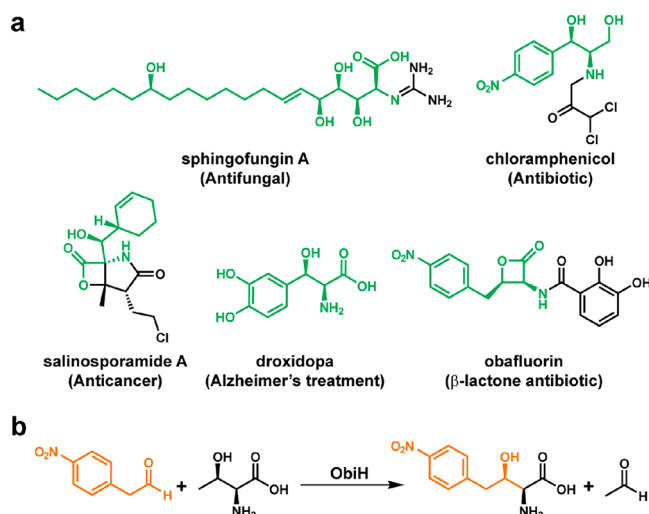


**Figure 1.**  $\beta$ -Hydroxy amino acids expand the amino acid repertoire. (a)  $\beta$ -Hydroxy amino acids and their derivatives (green) found in nature and in major pharmaceuticals. (b) Native L-threonine transaldolase reaction catalyzed by ObiH. (3R)- $\beta$ -Hydroxy-*p*-nitro-L-homophenylalanine is synthesized from *p*-nitrophenylacetaldehyde (orange) and L-threonine (black).

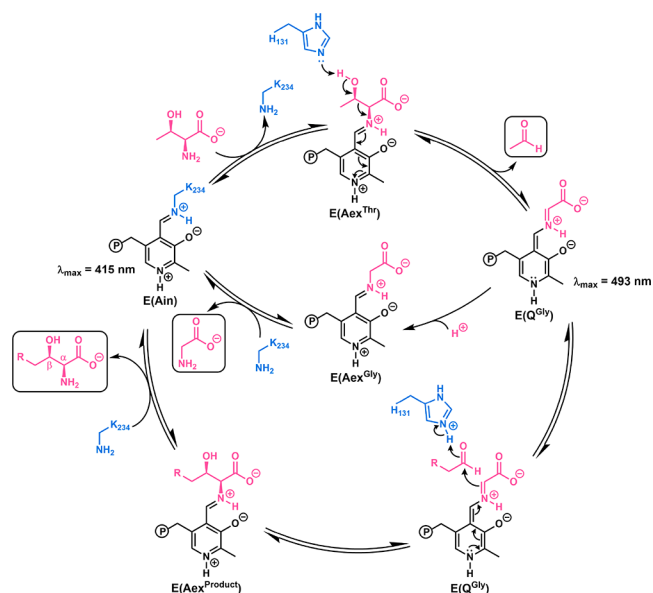
the nonheme Fe-dependent hydroxylation of homotyrosine in the biosynthesis of echinocandins.<sup>11</sup> The more common biosynthetic strategy, however, is for an amino acid to be loaded onto a nonribosomal peptide synthetase (NRPS), whereupon a P450 enzyme catalyzes C $\beta$  hydroxylation of an aminoacyl-S-enzyme intermediate en route to a peptide natural product.<sup>12–15</sup> Both of these biosynthetic strategies adds the hydroxyl group after assembly of the carbon backbone of a precursor amino acid. In contrast, there is a remarkable set of pyridoxal-5'-phosphate (PLP) dependent enzymes, L-threonine transaldolases (LTTAs), that catalyze retroaldol cleavage of L-threonine (Thr) and a subsequent aldol-like addition into an aldehyde to form a new side chain, setting the stereochemistry of the C $\beta$ -OH group (Figure 1b). The first LTTA to be discovered was the fluorothreonine transaldolase (FTA) from *Streptomyces cattleya*, which forms 4-fluoro-threonine from L-threonine and fluoroacetaldehyde.<sup>16</sup> Nucleoside antibiotics can also be formed through the action of LTTAs that transpose the side chain of Thr with the C5' aldehyde of a nucleoside.<sup>17,18</sup> Recently, two groups discovered in parallel that an LTTA, ObiH, reacts with *p*-nitrophenylacetaldehyde en route to obafuorin, a  $\beta$ -lactone aminoacyl tRNA synthetase inhibitor (Figure 1b).<sup>19–21</sup>

The mechanism of LTTA enzymes has not been studied in detail, and no structures are available. A mechanism has been proposed based on analogy to the homologous Thr aldolase (LTA) and serine hydroxymethyltransferase (SHMT) enzymes, which perform related transformations.<sup>22</sup> LTTAs catalyze the thermodynamically favorable breakdown of Thr into glycine (Gly) and acetaldehyde (Figure S1). This reaction begins with covalent capture of Thr as an external aldimine with PLP, E(Aex<sup>Thr</sup>).<sup>23</sup> The enzyme orients the side chain of Thr such that it is periplanar to the  $\pi$  system of the cofactor, in accordance with Dunathan's stereoelectronic hypothesis.<sup>24,25</sup> Retroaldol cleavage is initiated by deprotonation of the hydroxyl side chain by a conserved histidine (His) residue that  $\pi$ -stacks with the cofactor, either directly or through a proton relay with water.<sup>23</sup> Cleavage of the C $\alpha$ -C $\beta$  bond

releases acetaldehyde, and the resultant C $\alpha$  carbanion is stabilized through resonance as a highly basic glyceryl quinonoid intermediate, E(Q<sup>Gly</sup>).<sup>23</sup> The glyceryl quinonoid is subsequently protonated to form the external aldimine of glycine, E(Aex<sup>Gly</sup>), which is released to complete the catalytic cycle (Figure S1). The LTA reaction can be reversed to run in the synthetic direction *in vitro* by adding excess glycine and aldehyde. These enzymes have been shown to form diverse  $\beta$ -hydroxy amino acids, setting two stereocenters in the process.<sup>23,26,27</sup> However, the reversibility of the reaction and its relatively modest selectivity lead to scrambling of the stereochemistry at the  $\beta$ -position, limiting synthetic utility.<sup>28–31</sup>

Alternatively, LTTAs cleanly form  $\beta$ -hydroxy amino acids *in vivo* using the same Thr starting material and PLP cofactor.<sup>32</sup> Although the molecular details have yet to be elucidated, it is believed that these enzymes function by intercepting a highly reactive E(Q<sup>Gly</sup>) intermediate (Scheme 1). Initial studies with

**Scheme 1.** Catalytic Mechanism of ObiH<sup>a</sup>



<sup>a</sup>The mechanism of ObiH catalysis with Thr and an aldehyde substrate (outer cycle) along with the disfavored shunt pathway (inner cycle). The PLP cofactor (black) is shown covalently bound either to the substrates/intermediates (pink) or to the relevant catalytic residues of the protein (blue).

the LTTAs demonstrate several promising features for synthetic applications. FTA and ObiH homologues have been shown to react with a variety of aliphatic and aromatic aldehydes.<sup>33,34</sup> However, the lack of structural information stymies our understanding of the LTTA mechanism and hinders targeted engineering approaches. Here, we describe mechanistic and structural characterization of ObiH, a model LTTA, to understand the unique reactivity of these enzymes.

## RESULTS

**Green-Light Irradiation of Purified ObiH Yields Highly Active Catalyst.** ObiH was heterologously expressed as a N-His construct in *E. coli*, as was previously described.<sup>20</sup> This procedure reliably yields ~250 mg of protein per liter of culture (Figure S2). Consistent with previous reports, this protein is pink in color, whereas other PLP-dependent enzymes are yellow.<sup>19,20,34</sup> The UV-vis spectrum of ObiH

shows a peak at 415 nm, characteristic of the covalently bound internal aldimine adduct E(Ain), as well as an additional peak at 515 nm that accounts for the pink color (Figure 2a). During

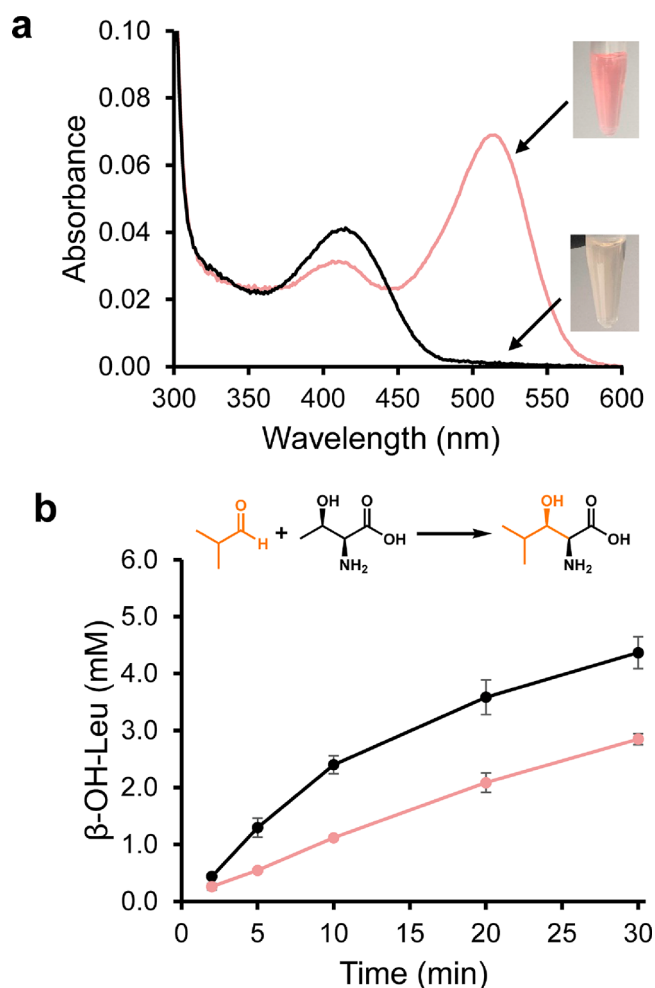


**Figure 2.** Effect of green light irradiation on ObiH catalytic states. (a) Absorbance spectra of natively purified ObiH (pink) and phototreated ObiH (black). Phototreatment results in the complete loss of the 515 nm species and increase in the E(Ain) peak at 415 nm. Images of ObiH stock solutions before and after phototreatment. (b) Comparison of product formation of (2S,3R)- $\beta$ -hydroxyisoleucine between as isolated ObiH (pink) and phototreated ObiH (black). The corresponding reaction is shown on top. Phototreated ObiH had a 2-fold increase in initial turnover rate compared to as-isolated enzymes.

our studies, it was observed that ObiH stock solutions slowly lost their pink color during the day. Intrigued by this unusual behavior, we placed a sample of purified ObiH in direct sunlight for 30 min, which transformed into a traditional yellow protein (Figure 2a). UV-vis analysis revealed complete abolishment of the 515 nm band and an increase at 415 nm. We also observed a decrease in the 515 nm species upon heating of ObiH at 37 °C (Figure S3). To minimize the possibility of stochastic protein aggregation at higher temperature, we relied on phototreatment to produce homogeneous ObiH. To further increase reproducibility, purified ObiH was exposed to an 8 W, green LED for 10 min on ice, which led to the rapid and reproducible photoablation of the 515 nm peak and a temporary increase at 340 nm (Figure S3). Over the course of several minutes, this 340 nm band decreased and the

415 nm band increased, indicative of a slow isomerization between the enolimine and ketoenamine forms of the cofactor, respectively.<sup>35</sup> While proton transfers are typically fast, we hypothesized that this apparent tautomerization is coupled to a slower exchange process, such as a conformational or oligomeric change. After isomerization of the 340 and 415 nm species, a small population of 515 nm species reformed. A second round of phototreatment removed the small amount of 515 nm species (Figure 2a). After storage at 4 °C overnight, phototreated ObiH samples equilibrated back to a mixture of states including the 515 nm species (Figure S3).

To assess whether the phototreatment increases the concentration of active enzymes and not some other species, we measured the initial velocity of ObiH with isobutyraldehyde before and after phototreatment. Gratifyingly, we observed an approximate 2-fold increase in the rate of product formation with the phototreated enzyme (Figure 2b). These data strongly suggest that heterologously expressed ObiH purifies as a mixture of chemically distinct states that can be photointerconverted and that the species absorbing at 515 nm is not catalytically active. Nevertheless, the phototreatment process afforded us the opportunity to cleanly assay the mechanistic properties of ObiH as a model LTTA.

#### ObiH Forms a Metastable PLP-Glycyl Quinonoid.

Previous steady-state kinetic analysis of ObiH established that the enzyme has a relatively high  $K_M$  for Thr, 40 mM.<sup>19</sup> We began our detailed mechanistic study by adding 100 mM Thr to ObiH and monitored the reaction by UV-vis spectroscopy. The addition of Thr resulted in an intense absorbance with  $\lambda_{max} = 493$  nm, characteristic of a PLP quinonoid adduct (Figure 3a). We assign this species as E(Q<sup>Gly</sup>), which is formed by retroaldol cleavage of a covalently bound PLP-Thr adduct, E(Aex<sup>Thr</sup>). We also performed this experiment with as-isolated enzymes (before phototreatment) and observed that the 515 nm peak was unchanged by reaction conditions. Further, as-isolated enzymes formed a less intense E(Q<sup>Gly</sup>) band, consistent with a lower population of the catalytically active enzyme (Figure S4).

The E(Q<sup>Gly</sup>) absorbance band increased for several minutes before reaching a maximum and slowly decayed over the course of several hours (Figure 3b). To further probe the kinetics of the formation and breakdown of this species, we repeated the experiment with varied concentrations of Thr. Increasing the concentration of Thr above 100 mM resulted in a similarly intense E(Q<sup>Gly</sup>) band, and lower concentrations of Thr significantly reduced the population of E(Q<sup>Gly</sup>) (Figure S5). We performed a global kinetic analysis of the time course for E(Q<sup>Gly</sup>) formation and decay across a range of Thr concentrations using a three-state kinetic model with reversible Thr binding and retro aldol cleavage, followed by an irreversible decay event. However, this simple model decisively failed to fit the data. Hence, additional studies that can substantiate a more sophisticated model will be required to account for the slow formation of E(Q<sup>Gly</sup>). Once formed, however, the reactivity of E(Q<sup>Gly</sup>) cleanly fit to a single exponential with a half-life of  $165 \pm 20$  min for concentrations  $\geq 100$  mM Thr (Figure S5). Given the time scale of this decay, many potential pathways may be responsible for the quenching of this species. We hypothesized that, in analogy to the distantly related LTA enzymes, E(Q<sup>Gly</sup>) reacted through simple protonation to form the glycyl external aldimine, E(Aex<sup>Gly</sup>).<sup>23</sup> Consistent with this hypothesis, kinetic analysis at lower pH showed a substantially faster quinonoid decay (Figure S6). In

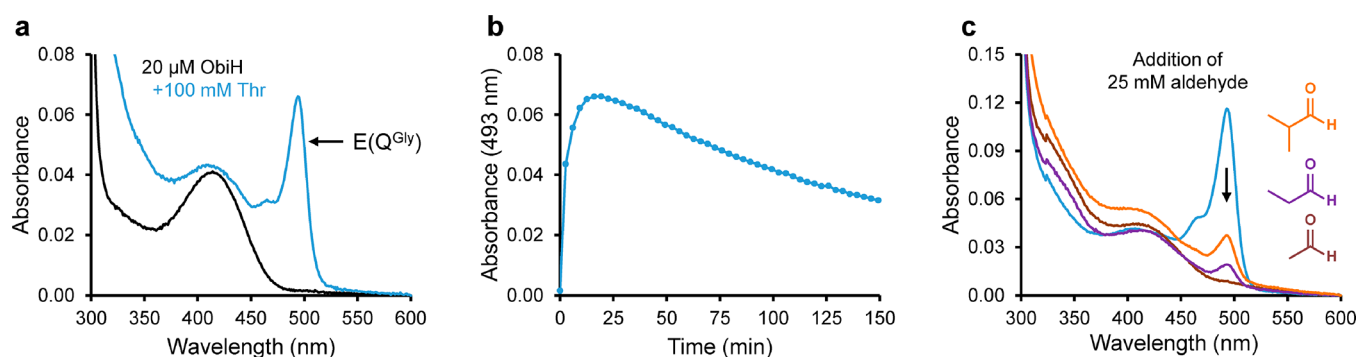


**Figure 3.** Spectroscopic characterization of ObiH catalytic intermediates. (a) Absorbance spectra of phototreated ObiH (black) and after addition of Thr (blue). Addition of Thr results in large peak at 493 nm,  $E(Q^{Gly})$ . (b) Plot of absorbance at 493 nm vs time after addition of Thr. The 493 nm peak increases rapidly before reaching a maximum with subsequent decay over hours. (c) On cycle reactivity of  $E(Q^{Gly})$  with aliphatic aldehydes. A representative absorbance spectrum (average absorption spectra between three experiments) of ObiH after addition of Thr is shown in blue. Subsequent addition of acetaldehyde (brown), propanal (purple), or isobutyraldehyde (orange) results in substantial reduction of the 493 nm peak.

the absence of an electrophile substrate, ObiH formed a small, but measurable amount of Gly, corresponding to <50 turnovers in 16 h.

To further confirm that Gly is formed through an ObiH-mediated process, we added Thr to ObiH to form a large population of  $E(Q^{Gly})$  and then reductively trapped the decay product as a secondary amine via the addition of  $NaBH_4$ . This reaction was monitored both spectrophotometrically and via UPLC-MS. Spectroscopic experiments showed depletion of the absorbing species in the range of 400–420 nm, indicating that the imines present  $E(Aex^{Thr})$ ,  $E(Aex^{Gly})$ , or unreacted  $E(Ain)$  were rapidly reduced by  $NaBH_4$  (Figure S7).

A new absorbance band at 340 nm appeared, consistent with formation of a reduced, secondary amine adduct.<sup>36</sup> However, the  $E(Q^{Gly})$  species (493 nm), which is electron-rich, was not immediately reduced by  $NaBH_4$  and decayed at a similar rate to reactions containing only Thr. The products of this reaction were monitored by UPLC-MS analysis and showed clear formation of a reduced glycol adduct (Figure S7). Notably, this experiment was performed with protein that had not undergone phototreatment and therefore retained the 515 nm absorbing species that can photoconvert to  $E(Ain)$ . Whereas  $E(Q^{Gly})$  was slowly depleted, presumably through an intermediate protonation step, the 515 nm band was completely resistant to reduction with  $NaBH_4$  (Figure, S7). While the above data show that  $E(Q^{Gly})$  is kinetically slow to react, they offer only indirect information on the thermodynamic stability of this intermediate. We therefore probed the effect of saturating Gly (1.0 M) on  $E(Ain)$  and observed no evidence of quinonoid formation, indicating that population of  $E(Q^{Gly})$  is not enabled by thermodynamic stabilization in the enzyme active site (Figure S8). Instead, these data establish that  $E(Q^{Gly})$  species is a kinetically trapped, high-energy intermediate.

**The ObiH Quinonoid Rapidly Reacts to Form  $\beta$ -Hydroxy Amino Acids.** The native electrophile in the ObiH reaction is *p*-nitrophenylacetaldehyde, which is generated via a thiamine-dependent decarboxylation from the corresponding  $\alpha$ -keto acid.<sup>19,20</sup> However, due to the inherent instability of arylacetaldehydes, we sought an alternative electrophile for our mechanistic studies. Recent experiments using a biocatalytic cascade showed ObiH, as well as its downstream enzymes in obafluorin biosynthesis, can react with a range of aliphatic and benzylic aldehydes.<sup>37</sup> While the synthetic utility of ObiH with

aromatic aldehydes has been recently reported,<sup>34,38</sup> we were drawn to the reaction with aliphatic aldehydes as mechanistic probes because they do not have confounding signals in their UV–vis spectra. We probed the on-path reactivity of ObiH via addition of reactive aldehyde to preformed  $E(Q^{Gly})$ . The addition of 25 mM acetaldehyde showed the rapid reaction of  $E(Q^{Gly})$  within the mixing time of the experiment (<20 s) and the persistence of a small, steady population of quinonoid (Figure 3c, brown). Because acetaldehyde reacts to reform the Thr starting material, a dynamic equilibrium is established. We repeated this experiment, titrating the active site with acetaldehyde and measuring the population of  $E(Q^{Gly})$ . These data fit cleanly to a single site binding isotherm, which indicates that acetaldehyde binds to  $E(Q^{Gly})$  with a  $K_D$  of  $430 \pm 15 \mu M$  (Figure S9).

We next probed the reaction of  $E(Q^{Gly})$  with different aliphatic aldehydes and measured the resulting steady-state quinonoid population. The addition of propanal resulted in a rapid loss of  $E(Q^{Gly})$ , but the steady-state population was higher than was observed in the acetaldehyde reaction (Figure S10). The addition of isobutyraldehyde differed from the previous two substrates and revealed that isobutyraldehyde reacts in at least two phases. Approximately half of the population of  $E(Q^{Gly})$  is depleted in the mixing time of the experiment. The remaining fraction reacts more slowly, reaching the steady state over the course of 20 min. Subsequent data establish that this aldehyde does react through a productive catalytic cycle to form a  $\beta$ -hydroxy amino acid product (*vide infra*). Other effects that occur on slow time scales, such as protonation to form Gly, however, confound further interpretation of these data.

To characterize the full catalytic cycle in action, we monitored product formation over time using isobutyraldehyde. UPLC-MS analysis of reactions with isobutyraldehyde showed a single peak corresponding to  $\beta$ -hydroxy-Leu, indicative of a highly diastereoselective reaction. The reaction proceeded slowly and reached a 71% yield after 24 h. To confirm the identity of the product, we performed an overnight preparative scale reaction on the 5 mmol scale using 0.04 mol % catalyst. Purification of the  $\beta$ -hydroxy-Leu proved to be challenging.  $\beta$ -hydroxy-Leu and Thr had similar retention times by C18 flash chromatography, which necessitated multiple rounds of chromatography to isolate the pure product and resulted in isolation of 141 mg of  $\beta$ -hydroxy-leucine,

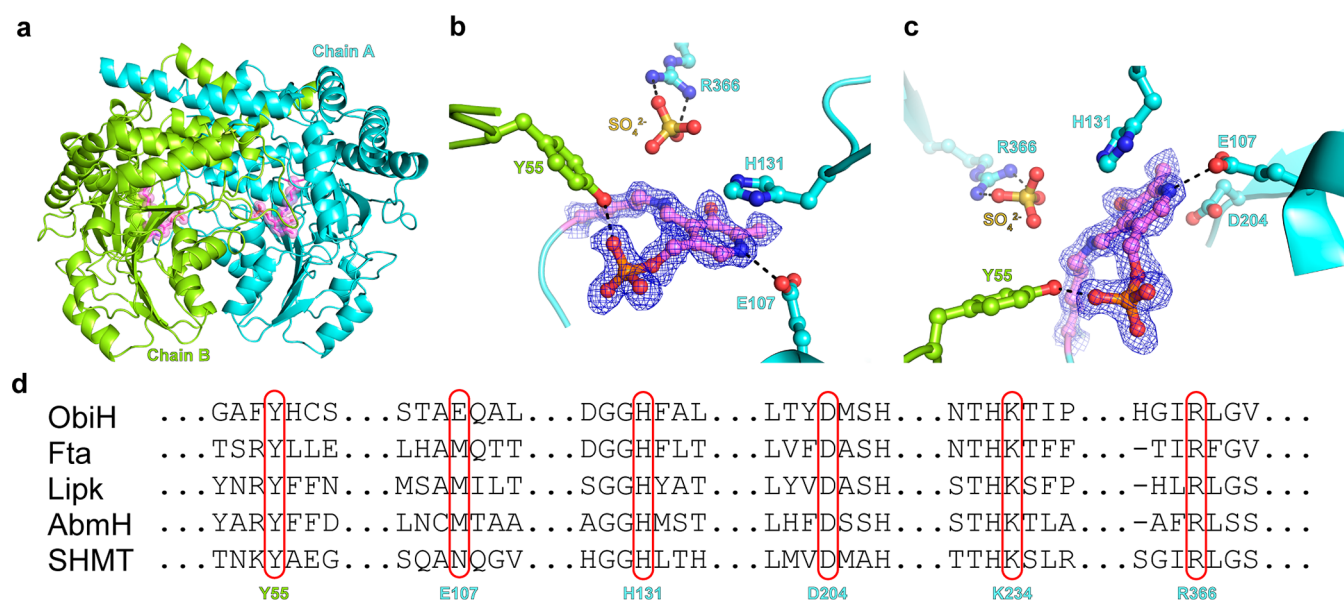


**Figure 4.** Structure of ObiH. (a) Cartoon representation of the overall structure of ObiH. Individual monomers are colored cyan (chain A) and lime (chain B). E(Ain) is shown as semitransparent pink spheres and sticks. (b) ObiH active site residues superimposed on the  $2F_o - DF_c$  electron density map (blue mesh,  $\sigma = 1.5$ ) are shown as sticks and colored as in part a. Hydrogen bonds are shown as black dashes. (c)  $45^\circ$  rotation of b. (d) Sequence alignment of example lTTAs and the evolutionarily related SHMT. Active site residues are highlighted with red boxes with numbering colors according to b and c. GenBank ID of ObiH is ARJ35753, FTA is WP\_014151017, Lipk is BAJ05887, AbmH is AVIS7436, and SHMT is AFJ20773.

corresponding to a 38% isolated yield. NMR analysis revealed a >98:2 diastereomeric ratio (dr) of syn/anti products. ObiH, like other fold type-I PLP dependent enzymes, is known to have exquisite selectivity for the 2S configuration.<sup>39,40</sup> Therefore, we assign this product as (2S,3R)- $\beta$ -hydroxy-Leu, consistent with other studies of ObiH selectivity.<sup>20</sup> To probe the reactivity of this amino acid with ObiH, we added 25 mM  $\beta$ -hydroxy-Leu and observed a low population of E(Q<sup>Gly</sup>) that formed slowly over the course of 30 min. These data demonstrate that the  $\beta$ -hydroxy-Leu product does not readily re-enter the catalytic cycle (Figure S11).

**ObiH Crystallizes with an Unanticipated Active Site Conformation.** To unravel the structural properties underpinning this unique reactivity, we crystallized N-His-ObiH to capture the enzyme in its internal aldimine state, E(Ain). High resolution, 1.66-Å, X-ray diffraction data were collected on crystals that retained the 515 nm species, as the pink color was maintained throughout the process. The structure was solved by molecular replacement with a distantly related serine hydroxymethyltransferase (PDB ID: 4OT8, 28.2% identity).<sup>41</sup> The asymmetric unit of the ObiH crystal was comprised of four protamers (two dimers) for a total of four unique observations of the active site. ObiH crystallized as a domain swapped homodimer, with an extension of the C-terminus forming the dimer interface. Such dimerization is consistent with other members of the fold-type I superfamily of PLP-dependent enzymes (Figure 4a).<sup>40</sup> Structural superposition of all non-hydrogen atoms of the four ObiH protamers shows that they are highly consistent (RMSD =  $0.47 \pm 0.06$  Å<sup>2</sup>). While the vast majority of the structure was rapidly built following common structural motifs, we were initially stymied by the density corresponding to a Cys-cisPro linkage in a  $\pi$ -bulge of an  $\alpha$ -helix (Figure S12). The carbonyl oxygen of Cys262 is just 2.9 Å away from the carbonyl of the *i*-4 residue, an otherwise strained conformation that appears to be stabilized by hydrogen bonds from each carbonyl to Arg99.

The ObiH active site lies at the dimer interface, with most of the residues contributed from a single subunit. The electron density is consistent with a typical E(Ain) state of the enzyme where the conserved Lys234 forms a Schiff's base adduct with the PLP cofactor (Figure 4b,c).<sup>42</sup> A molecule of sulfate is bound in the active site with the same orientation in all four subunits and forms a salt bridge with Arg366. Such complexes with a sulfate or phosphate are common among PLP-dependent enzymes and often correspond to the carboxylate-binding motif within the active site.<sup>42–45</sup> The pyridine ring of PLP is  $\pi$ -stacked with His131, and the PLP phosphate is buried with an intricate web of hydrogen bonds, including two to Tyr55 and Asn268 from the partner subunit. A multiple sequence alignment reveals that Lys234, Arg366, His131, and Tyr55 are highly conserved across biochemically characterized lTTAs (Figure 4d).

Another highly conserved residue in this family of enzymes is the residue that hydrogen bonds to the pyridine nitrogen of the cofactor, Asp204.<sup>40</sup> Ion pairing with the pyridinium moiety enforces protonation of the cofactor, thereby increasing its electrophilicity. However, the universally conserved Asp residue appeared to be tucked under the pyridine ring, and instead, Glu107 is in position to form a salt bridge with the cofactor (Figure 4c). Mutation of the residue that H-bonds to the pyridine of PLP is known to occur within the fold type II PLP-dependent enzymes, but each residue is highly conserved among its family members.<sup>42,46,47</sup> However, Glu107 is not conserved between lTTAs, and we speculated this residue might not be essential for ObiH function (Figure 4d). In order to determine which residue was engaging the cofactor during catalysis, we made substantial efforts to trap an ObiH external aldimine. Despite successful crystal growth and diffraction, the crystals were excessively twinned, and no clear picture of the active site emerged. We therefore sought to use computational methods to build an atomic model of ObiH external aldimine,

E(Aex<sup>Thr</sup>), to assess whether a conformational rearrangement involving Glu107 and Asp204 might be occurring.

**Simulations Show Active Site Dynamics.** We first conducted 110 ns molecular dynamics (MD) simulations of the ObiH dimer in the E(Ain) state. Trajectories were run in triplicate and were well equilibrated after 10 ns of simulation time. These initial 10 ns were excluded from subsequent analysis. Measurements from both monomers were combined, effectively doubling the active site sampling frequency across the combined 300 ns simulation time. Initial visual inspection of the simulation results revealed that a loop region spanning Tyr55 to Pro71 had moved significantly during the course of the simulation. Per-residue root-mean-square fluctuation (RMSF) analysis of the backbone atoms shows this loop region, which coincides with the putative substrate access channel, is one of the most mobile regions of the protein (Figure S13). These results were not surprising, as this region in the crystal structure was largely void of secondary structure.

To probe the dynamics of the active site, we used H-bonding analysis of the residues near the PLP cofactor to assess which residue H-bonded to the pyridine nitrogen (PLP-N1) during the course of the simulations. This analysis revealed that both Glu107 and Asp204 can H-bond to the cofactor, but that Glu107 was more than twice as likely to engage the cofactor (Table S2). This population distribution was consistent with H-bond lifetime analysis, which indicated that the H-bond to Glu107 is more than 4 times as persistent as that of Asp204 (Figure S14). These measurements agreed with the crystallographic observation that Glu107 is the main H-bonding acceptor in the resting state of the catalyst.

We next turned our attention to simulations of the ObiH dimer in the chemical state that immediately precedes the retroaldol cleavage, E(Aex<sup>Thr</sup>). Prior literature has shown that PLP-dependent enzymes often undergo active site rearrangements upon substrate binding, including motion of the cofactor.<sup>41,42,48</sup> Although the residue that H-bonds to the cofactor is usually consistent during catalysis, we speculated that ObiH could facilitate exchange of Glu107 for Asp204. We used the cofactor orientation from an analogous E(Aex<sup>Ser</sup>) state from L-serine hydroxymethyltransferase (SHMT; PDB ID: 4OT8) as the template for initial placement of the E(Aex<sup>Thr</sup>) in ObiH.<sup>41</sup> RMSF analysis showed that the flexible Tyr55-Pro71 loop region becomes even more mobile upon external aldimine formation. This loop contains a six residue insertion compared to a structurally similar SHMT (PDB: 1KL2), which may explain the high degree of mobility observed (Figure S13c). A neighboring loop, Glu355-His363, is shorter compared to SHMT. These two loop regions directly interact with folate in SHMT, and the modifications present in ObiH may contribute to the aldehyde specificity of the enzyme. Active site conformations with H-bonds to both Glu107 and Asp204 were again well-sampled during the simulations. In contrast to E(Ain), Asp204 H-bonded to the cofactor at twice the frequency of Glu107 in the E(Aex<sup>Thr</sup>) state, and these H-bonds had similar lifetimes (Table S2).

To form a clearer picture of the different conformational landscapes of ObiH in the E(Ain) and E(Aex<sup>Thr</sup>) states, we used free energy surface (FES) analysis.<sup>49</sup> Due to the high degree of mobility in the Tyr55-Pro71 loop and its proximity to the active site, we selected the distance from Trp68 to Phe132 as one measurement criterion. Additionally, we chose the center-to-center distance of His131 to the cofactor pyridine

ring. His131  $\pi$ -stacks with the cofactor in the crystal structure and is in a prime position to act as a catalytic base to initiate retroaldol cleavage. For simulations of E(Ain), the regions of the landscape sampled by the protein while H-bonded to Glu107 are distinct from those sampled during H-bonding to Asp204 (Figure S15).

We applied the same FES analysis to simulations of E(Aex<sup>Thr</sup>) and observed a dramatic shift in the conformational landscape. The Asp204 H-bond was sampled at a higher frequency and across a wider region of the conformational landscape. However, it was not immediately clear whether any of the sampled regions corresponded to a potentially catalytically active state. We used the presence of a H-bond between His131 and the side chain hydroxyl group of E(Aex<sup>Thr</sup>) as an indicator of a catalytic state, as His131 is the evolutionarily conserved base for retroaldol cleavage (Figure 4d). We found that the FES where His131 adopted this state coincided with regions where Asp204 was H-bonded to the cofactor (Figure S16), strongly suggesting that Asp204 is the residue that engages the cofactor during retroaldol cleavage. There was still a diverse conformational space where each of the potential catalytic His131 and Asp204 interactions were satisfied. To further narrow our search for a catalytic pose, we searched for orientations where the substrate carboxylate was also engaged in a salt bridge with Arg366, as previous structural studies have shown this interaction is conserved across LTAs and SHMTs (Figure 5, Figure S17). This snapshot of ObiH E(Aex<sup>Thr</sup>) satisfies each plausible interaction of a catalytically productive pose and may be useful for future studies.

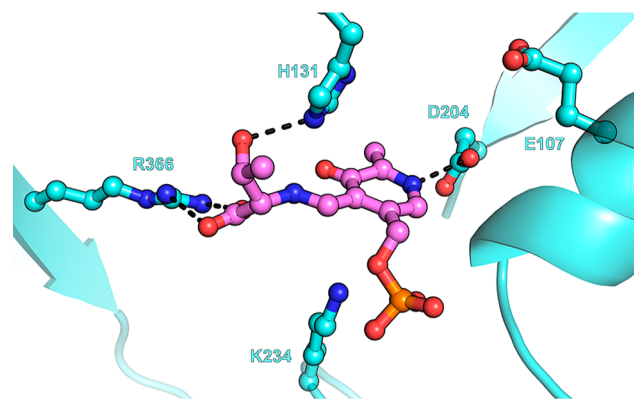


**Figure 5.** Molecular dynamics simulation of E(Aex<sup>Thr</sup>). E(Aex<sup>Thr</sup>) shown in pink. ObiH shown in cyan. Hydrogen bonds that are proposed to facilitate substrate binding and catalysis are shown as black dashes.

**Asp204 Is Essential for Catalysis.** To experimentally validate the insights gained from molecular dynamic simulations and bioinformatics analyses, we performed biochemical characterization of His131, Glu107, and Asp204 variants. Rather than the traditional alanine scan approach to probe the “importance” of a residue, we screened a site-saturation mutagenesis library at His131 for retention of function with biphenyl-4-carboxaldehyde, as the products were well-behaved on UPLC-MS. The native ObiH enzyme, bearing His131, possessed the highest activity under the screening conditions (Figure S18). The only residue that supported any catalytic function other than His was Gly, which may allow water to enter the active site and rescue function. This

experiment supports our observation from crystallographic and MD simulation that His131 is the catalytic base.

Next, we screened a site-saturation mutagenesis library at Glu107. Similar to His131, the native ObiH enzyme, bearing Glu107, possessed the highest activity. Unlike His131, however, many other variants retained catalytic activity (Figure S18). To further probe the role of Glu107, we expressed and purified the conservative E107Q variant, which has a similar steric profile to the native residue but cannot form an ion pair with the pyridinium nitrogen. This protein was pink in color and behaved similarly to wild type protein upon phototreatment (Figure S19). Spectroscopic analysis affirmed that ObiH-E107Q binds PLP and, upon the addition of Thr, enters the catalytic cycle to form a metastable quinonoid that goes on to react with propanal (Figure 6).

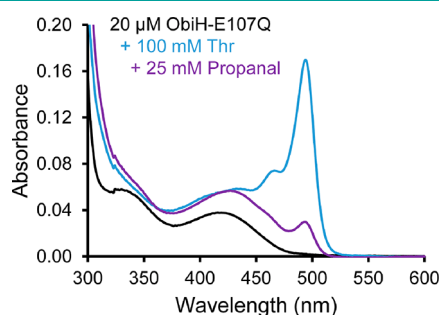


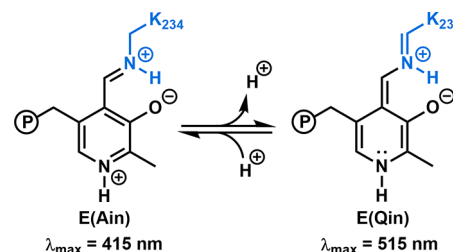
**Figure 6.** Spectroscopic characterization of ObiH-E107Q. Absorbance spectra of phototreated ObiH-E107Q (black) and after addition of Thr (blue). Addition of Thr results in a large peak at 493 nm, E(Q<sup>Gly</sup>). Subsequent addition of propanal (purple) results in substantial reduction of the 493 nm peak. These spectral features of ObiH-E107Q are similar to wt-ObiH.

In stark contrast, saturation mutagenesis at the evolutionarily conserved Asp204 position was catastrophic, and only the wild-type enzyme retained activity (Figure S18). We attempted to further probe the contribution of Asp204 through study of the conservative D204N variant. This protein aggregated during purification and was stable only at low concentrations. The purified ObiH-D204N was colorless, and UV-vis analysis revealed evidence of only trace PLP binding (Figure S19). These experiments unambiguously demonstrate that Asp204, not Glu107, is essential for efficient cofactor binding and enforces protonation at PLP-N1 to enable the unique transaldolase activity of this enzyme.

## DISCUSSION

**ObiH May Form an Internal Quinonoid.** One of the most striking observations about ObiH, by us and others,<sup>20,37</sup> is the beautiful and uncommon pink color of the heterologously expressed protein. UV-vis analysis indicates the presence of an adduct that absorbs at 515 nm. The  $\lambda_{\max}$  of this species is itself highly informative and suggests formation of an extended chromophore with the PLP-cofactor, such as a quinonoid. Indeed, the 515 nm band was originally hypothesized to arise from a small population of tightly bound glycol quinonoid, E(Q<sup>Gly</sup>).<sup>20</sup> However, the addition of Thr yields a quinonoid with a distinct  $\lambda_{\max}$  and the shoulder at 515 nm remains, ruling out E(Q<sup>Gly</sup>) as a copurifying species (Figure S4). Instead, we hypothesize that this unusual spectral feature arises from a small population of a deprotonated Schiff base adduct, an internal quinonoid E(Qin) (Scheme 2). There

## Scheme 2. Formation of Protein-Bound PLP Quinonoid<sup>a</sup>



<sup>a</sup>Deprotonation of lysine at Cε of the internal aldimine, E(Ain), could promote the formation of the internal quinonoid, E(Qin).

are several lines of evidence that support this assignment. Through an as-yet-unknown process, light abolishes this species and increases the concentration of the E(Ain), establishing that the 515 nm species is a PLP adduct and not some trace contaminant (Figure 2a). Such reactivity is uncommon, and doubtless will inspire further study, but is consistent with a previous report that light can alter the pK<sub>a</sub> of PLP intermediates.<sup>36</sup> We show that the 515 nm species can interconvert to a catalytically active state through both photochemical and thermal means (Figure S3). However, the 515 nm band was inert to reduction with NaBH<sub>4</sub>, indicating that it is electron rich (Figure S7). Last, the structure of ObiH was determined from pink crystals, and despite the high, 1.66-Å resolution of the data, no trace of a contaminating chromophore was observed, consistent with an isosteric modification (Figure 4b).

Each of the above lines of evidence support the assignment of the 515 nm band as E(Qin), but none suggest why this species arises in the first place. Detailed pre-steady-state kinetic experiments conclusively established that the native function of ObiH involves formation of E(Q<sup>Gly</sup>) (Figure 3a). No trace of E(Q<sup>Gly</sup>) is formed upon the addition of Gly to solution, indicating that this intermediate is highly basic (Figure S8). However, this species persists for hours in the absence of an electrophile and is therefore kinetically shielded from protonation. We speculate that these same features that underlie the catalytic reactivity of ObiH may also be responsible for stabilization of an E(Qin) state. While this is a parsimonious explanation, many details of E(Qin) formation remain unclear. What is the role of light and temperature in facilitating the apparent protonation of this species? Is this chemistry unique to ObiH, or common among LTTA enzymes? These and other questions leave fertile ground for future study.

**Structure Guided MD Simulations and Mutagenesis Reveal the Role of Active Site Residues.** Crystallographic structures are highly information-rich and often lead to key mechanistic insights. However, they provide a handful of snapshots of the protein in a solid, crystalline environment that does not always reflect behavior in solution. Further, even high-resolution models can only capture states that are <1.0 kcal/mol from the thermodynamic minimum. As described in the Results, we found that N-His-ObiH crystallized in a highly unexpected conformation, with Glu107 H-bonded to the pyridinium moiety of the cofactor instead of the evolutionarily conserved Asp204. MD simulations of E(Ain) revealed significant conformational heterogeneity of a loop adjacent to the active site and indicated that a H-bond with either of the two residues was likely, with Glu107 preferred. Hence, even

the small energetic bias induced by asymmetric packing forces in the crystalline lattice could reasonably alter this equilibrium, resulting in the observed crystallographic state (Figure 4b). In contrast, MD simulation of E(Aex<sup>Thr</sup>) revealed that Asp204 is the predominant residue that H-bonds with PLP-N1. These data align with strong literature precedence from related serine hydroxymethyltransferase (SHMT) and LTA enzymes.<sup>41</sup> Combined with our mutagenesis and spectroscopic studies of ObiH and its E107Q variant (Figure 6), these results affirm that Asp204, and not Glu107, plays a key role in facilitating quinonoid formation. Given the conservation of Asp204 among LTTA enzymes, we anticipate its role in catalysis will be a general feature among this enzyme family (Figure 4d).

**The Persistence of E(Q<sup>Gly</sup>) Enables Biocatalytic Access to  $\beta$ -Hydroxy-Amino Acids.** Quinonoid intermediates are nearly ubiquitous among PLP-dependent enzymes.<sup>50</sup> Some enzymes form thermodynamically stable quinonoids simply by binding substrates, products, or analogs thereof.<sup>51–53</sup> For example, the addition of Gly to LTA enzymes results in formation of a thermodynamically stable quinonoid.<sup>54</sup> Other enzymes only transiently form quinonoids, and rapid kinetic analysis is needed to observe them.<sup>55</sup> ObiH is exceptional, in that it forms a large population of thermodynamically unstable quinonoid. Were protonation and release of Gly to occur, this would be thermodynamically favored *in vivo*, precluding biosynthesis of new  $\beta$ -hydroxy amino acids. Hence, there is a selective pressure to kinetically shield E(Q<sup>Gly</sup>) from protonation. This intermediate rapidly reacts when an aldehyde substrate is added (Figure 3c). This scenario also explains an otherwise perplexing observation made by previous studies of LTTA enzymes that Gly does not effectively enter the catalytic cycle: the E(Q<sup>Gly</sup>) is thermodynamically unstable in LTTA active sites.

While the focus of the present work is on structure and mechanism, experiments with the native *p*-nitrophenylacetaldehyde substrate were hindered by the instability of this compound in water. We therefore sought to probe the ObiH reaction with an  $\alpha$ -branched isobutyraldehyde substrate that forms (2*S*,3*R*)- $\beta$ -hydroxy-Leu. Synthesis of this desirable amino acid analog previously required multistep methods, which are vastly simplified with this biocatalytic route.<sup>56,57</sup> Notably, initial velocity studies showed ObiH turns over isobutyraldehyde at a rate of 12 min<sup>-1</sup> (Figure 2b). Were the competing protonation pathway facile, formation of  $\beta$ -hydroxy-Leu would be severely limited. Hence, the long lifetime of the E(Q<sup>Gly</sup>) intermediate enables reactivity with non-native aldehyde substrates.

We envision this mechanistic and structural information will spur future application of ObiH and other LTTA enzymes for preparative scale biocatalysis. Coupled enzyme reactions have shown that ObiH can react with phenylacetaldehydes, as well as a handful of simpler aliphatic aldehydes.<sup>37</sup> Studies have also revealed that ObiH and its homologues can react with over a dozen aromatic aldehydes.<sup>37,38</sup> Unlike the LTAs, several of the resulting phenyl serine analogs can be formed with both high yield and excellent dr. Recently, the ObiH homologue, P<sub>S</sub>LTTA (99% sequence identity), was engineered for improved yield and selectivity en route to (2*S*,3*R*)-*p*-methylsulfonylphenylserine.<sup>38</sup> These authors reported a double mutant, N35S/C57N, that increased activity with the corresponding aldehyde by 8-fold. The structure and MD simulations of ObiH reported here reveal that Asn35 is in the active site of the enzyme and that Cys57 is within a highly mobile loop. Although this variant has

relatively low conversion with other substrates, the availability of structural data may facilitate targeted engineering approaches to further improve the catalyst. This information, combined with the high expression titer of ObiH and its stability over months at -80 °C, make this enzyme highly attractive for future biocatalytic applications.

## ■ ASSOCIATED CONTENT

### Supporting Information

The Supporting Information is available free of charge at <https://pubs.acs.org/doi/10.1021/acschembio.0c00753>.

Complete materials and methods as well as supplemental figures and crystallographic information (PDF)

## ■ AUTHOR INFORMATION

### Corresponding Author

Andrew R. Buller – Department of Chemistry and Department of Biochemistry, University of Wisconsin–Madison, Madison, Wisconsin 53706, United States; [orcid.org/0000-0002-9635-4844](https://orcid.org/0000-0002-9635-4844); Email: [arbuller@wisc.edu](mailto:arbuller@wisc.edu)

### Authors

Prasanth Kumar – Department of Chemistry, University of Wisconsin–Madison, Madison, Wisconsin 53706, United States; [orcid.org/0000-0001-6175-4883](https://orcid.org/0000-0001-6175-4883)

Anthony Meza – Department of Biochemistry, University of Wisconsin–Madison, Madison, Wisconsin 53706, United States

Jonathan M. Ellis – Department of Chemistry, University of Wisconsin–Madison, Madison, Wisconsin 53706, United States

Grace A. Carlson – Department of Chemistry, University of Wisconsin–Madison, Madison, Wisconsin 53706, United States

Craig A. Bingman – Department of Biochemistry, University of Wisconsin–Madison, Madison, Wisconsin 53706, United States

Complete contact information is available at: <https://pubs.acs.org/doi/10.1021/acschembio.0c00753>

### Author Contributions

<sup>§</sup>These authors contributed equally.

### Funding

This work was supported by the Office of the Vice Chancellor for Research and Graduate Education at the University of Wisconsin—Madison with funding from the Wisconsin Alumni Research Foundation and the NIH DP2-GM137417 to A.R.B.; Morgridge Institute for Research – Metabolism Theme Fellowship to P.K.; NIH Chemistry–Biology Interface Training Grant T32-GM008505 to A.M.; and NIH Biotechnology Training Grant T32-GM008349 to J.M.E. The Bruker AVANCE III-500 NMR spectrometers were supported by the Bender Fund. Use of the Advanced Photon Source was supported by the U.S. Department of Energy, Office of Science, Office of Basic Energy Sciences, under Contract No. W-31-109-Eng-38.

### Notes

The authors declare no competing financial interest.

## ACKNOWLEDGMENTS

We acknowledge the invaluable support, assistance, and advice from our colleagues in the Buller lab. We thank R. Trachman for helpful discussion and comments on the manuscript. We are grateful to the Yoon group for the use of their LEDs.

## ABBREVIATIONS

LTTAs, L-Threonine transaldolases; nCAAs, noncanonical amino acids; NRPS, nonribosomal peptide synthetase; PLP, pyridoxal-5'-phosphate; Thr, L-threonine; FTA, fluorothreonine transaldolase; lTA, Thr aldolase; SHMT, serine hydroxymethyltransferase; Gly, glycine; E(Aex<sup>Thr</sup>), Thr external aldimine; E(Q<sup>Gly</sup>), glycol quinonoid; E(Aex<sup>Gly</sup>), Gly external aldimine; E(Ain), internal aldimine; dr, diastereomeric ratio; MD, molecular dynamics; RMSF, root-mean-square fluctuation; PLP-N1, pyridine nitrogen; FES, free energy surface; E(Qin), internal quinonoid

## REFERENCES

- (1) Blaskovich, M. A. T. (2016) Unusual Amino Acids in Medicinal Chemistry. *J. Med. Chem.* 59 (24), 10807–10836.
- (2) Walsh, C. T., O'Brien, R. V., and Khosla, C. (2013) Nonproteinogenic Amino Acid Building Blocks for Nonribosomal Peptide and Hybrid Polyketide Scaffolds. *Angew. Chem., Int. Ed.* 52 (28), 7098–7124.
- (3) Zweerink, M. M., Edison, A. M., Wells, G. B., Pinto, W., and Lester, R. L. (1992) Characterization of a Novel, Potent, and Specific Inhibitor of Serine Palmitoyltransferase. *J. Biol. Chem.* 267 (35), 25032–25038.
- (4) Feling, R. H., Buchanan, G. O., Mincer, T. J., Kauffman, C. A., Jensen, P. R., and Fenical, W. (2003) Salinosporamide A: A Highly Cytotoxic Proteasome Inhibitor from a Novel Microbial Source, a Marine Bacterium of the New Genus Salinospora. *Angew. Chem., Int. Ed.* 42 (3), 355–357.
- (5) Shevach, E. M. (1985) The Effects of Cyclosporin A on the Immune System. *Annu. Rev. Immunol.* 3 (1), 397–423.
- (6) Miller, M. J. (1986) Hydroxamate Approach to the Synthesis of  $\beta$ -Lactam Antibiotics. *Acc. Chem. Res.* 19 (2), 49–56.
- (7) Tanner, D. (1994) Chiral Aziridines—Their Synthesis and Use in Stereoselective Transformations. *Angew. Chem., Int. Ed. Engl.* 33 (6), 599–619.
- (8) Desimoni, G., Faita, G., and Quadrelli, P. (2003) Pyridine-2,6-Bis(Oxazolines), Helpful Ligands for Asymmetric Catalysts. *Chem. Rev.* 103 (8), 3119–3154.
- (9) Goldstein, D. S. (2006) L-Dihydroxyphenylserine (L-DOPS): A Norepinephrine Prodrug. *Cardiovasc. Drug Rev.* 24 (3–4), 189–203.
- (10) van Wageningen, A. M., Kirkpatrick, P. N., Williams, D. H., Harris, B. R., Kershaw, J. K., Lennard, N. J., Jones, M., Jones, S. J., and Solenberg, P. J. (1998) Sequencing and Analysis of Genes Involved in the Biosynthesis of a Vancomycin Group Antibiotic. *Chem. Biol.* 5 (3), 155–162.
- (11) Jiang, W., Cacho, R. A., Chiou, G., Garg, N. K., Tang, Y., and Walsh, C. T. (2013) EcdGHK Are Three Tailoring Iron Oxygenases for Amino Acid Building Blocks of the Echinocandin Scaffold. *J. Am. Chem. Soc.* 135 (11), 4457–4466.
- (12) Recktenwald, J., Shawky, R., Puk, O., Pfennig, F., Keller, U., Wohlleben, W., and Pelzer, S. (2002) Nonribosomal Biosynthesis of Vancomycin-Type Antibiotics: A Heptapeptide Backbone and Eight Peptide Synthetase Modules. *Microbiology* 148 (4), 1105–1118.
- (13) Puk, O., Bischoff, D., Kittel, C., Pelzer, S., Weist, S., Stegmann, E., Süssmuth, R. D., and Wohlleben, W. (2004) Biosynthesis of Chloro- $\beta$ -Hydroxytyrosine, a Nonproteinogenic Amino Acid of the Peptidic Backbone of Glycopeptide Antibiotics. *J. Bacteriol.* 186 (18), 6093–6100.
- (14) Cryle, M. J., Meinhart, A., and Schlichting, I. (2010) Structural Characterization of OxyD, a Cytochrome P450 Involved in  $\beta$ -Hydroxytyrosine Formation in Vancomycin Biosynthesis. *J. Biol. Chem.* 285 (32), 24562–24574.
- (15) Chen, H., Thomas, M. G., O'Connor, S. E., Hubbard, B. K., Burkart, M. D., and Walsh, C. T. (2001) Aminoacyl-S-Enzyme Intermediates in  $\beta$ -Hydroxylations and  $\alpha,\beta$ -Desaturations of Amino Acids in Peptide Antibiotics. *Biochemistry* 40 (39), 11651–11659.
- (16) Murphy, C. D., O'Hagan, D., and Schaffrath, C. (2001) Identification of a PLP-Dependent Threonine Transaldolase: A Novel Enzyme Involved in 4-Fluorothreonine Biosynthesis in *Streptomyces Cattlea*. *Angew. Chem., Int. Ed.* 40 (23), 4479–4481.
- (17) Barnard-Britson, S., Chi, X., Nonaka, K., Spork, A. P., Tibrewal, N., Goswami, A., Pahari, P., Ducho, C., Rohr, J., and Van Lanen, S. G. (2012) Amalgamation of Nucleosides and Amino Acids in Antibiotic Biosynthesis: Discovery of an l-Threonine:Uridine-5'-Aldehyde Transaldolase. *J. Am. Chem. Soc.* 134 (45), 18514–18517.
- (18) Ushimaru, R., and Liu, H. (2019) Biosynthetic Origin of the Atypical Stereochemistry in the Thioheptose Core of Albomycin Nucleoside Antibiotics. *J. Am. Chem. Soc.* 141 (6), 2211–2214.
- (19) Scott, T. A., Heine, D., Qin, Z., and Wilkinson, B. (2017) An L-Threonine Transaldolase Is Required for L-Threo- $\beta$ -Hydroxy- $\alpha$ -Amino Acid Assembly during Obafluorin Biosynthesis. *Nat. Commun.* 8 (1), 15935.
- (20) Schaffer, J. E., Reck, M. R., Prasad, N. K., and Wenczewicz, T. A. (2017)  $\beta$ -Lactone Formation during Product Release from a Nonribosomal Peptide Synthetase. *Nat. Chem. Biol.* 13 (7), 737–744.
- (21) Scott, T. A., Batey, S. F. D., Wiencsek, P., Chandra, G., Alt, S., Francklyn, C. S., and Wilkinson, B. (2019) Immunity-Guided Identification of Threonyl-TRNA Synthetase as the Molecular Target of Obafluorin, a  $\beta$ -Lactone Antibiotic. *ACS Chem. Biol.* 14 (12), 2663–2671.
- (22) Contestabile, R., Paiardini, A., Pascarella, S., Di Salvo, M. L., D'Aguzzo, S., and Bossa, F. (2001) L-Threonine Aldolase, Serine Hydroxymethyltransferase and Fungal Alanine Racemase: A Subgroup of Strictly Related Enzymes Specialized for Different Functions. *Eur. J. Biochem.* 268 (24), 6508–6525.
- (23) Di Salvo, M. L., Remesh, S. G., Vivoli, M., Ghatge, M. S., Paiardini, A., D'Aguzzo, S., Safo, M. K., and Contestabile, R. (2014) On the Catalytic Mechanism and Stereospecificity of *Escherichia Coli* l-Threonine Aldolase. *FEBS J.* 281 (1), 129–145.
- (24) Dunathan, H. C. (1966) Conformation and Reaction Specificity in Pyridoxal Phosphate Enzymes. *Proc. Natl. Acad. Sci. U. S. A.* 55 (4), 712–716.
- (25) Kielkopf, C. L., and Burley, S. K. (2002) X-Ray Structures of Threonine Aldolase Complexes: Structural Basis of Substrate Recognition. *Biochemistry* 41 (39), 11711–11720.
- (26) Steinreiber, J., Schürmann, M., Wolberg, M., Van Assema, F., Reisinger, C., Fesko, K., Mink, D., and Griengl, H. (2007) Overcoming Thermodynamic and Kinetic Limitations of Aldolase-Catalyzed Reactions by Applying Multienzymatic Dynamic Kinetic Asymmetric Transformations. *Angew. Chem., Int. Ed.* 46 (10), 1624–1626.
- (27) Steinreiber, J., Fesko, K., Mayer, C., Reisinger, C., Schürmann, M., and Griengl, H. (2007) Synthesis of  $\gamma$ -Halogenated and Long-Chain  $\beta$ -Hydroxy- $\alpha$ -Amino Acids and 2-Amino-1,3-Diols Using Threonine Aldolases. *Tetrahedron* 63 (34), 8088–8093.
- (28) Fesko, K., Strohmeier, G. A., and Breinbauer, R. (2015) Expanding the Threonine Aldolase Toolbox for the Asymmetric Synthesis of Tertiary  $\alpha$ -Amino Acids. *Appl. Microbiol. Biotechnol.* 99 (22), 9651–9661.
- (29) Kimura, T., Vassilev, V. P., Shen, G.-J., and Wong, C.-H. (1997) Enzymatic Synthesis of  $\beta$ -Hydroxy- $\alpha$ -Amino Acids Based on Recombinant d- and l-Threonine Aldolases. *J. Am. Chem. Soc.* 119 (49), 11734–11742.
- (30) Fesko, K. (2016) Threonine Aldolases: Perspectives in Engineering and Screening the Enzymes with Enhanced Substrate and Stereo Specificities. *Appl. Microbiol. Biotechnol.* 100 (6), 2579–2590.
- (31) Chen, Q., Chen, X., Feng, J., Wu, Q., Zhu, D., and Ma, Y. (2019) Improving and Inverting C  $\beta$  -Stereoselectivity of Threonine

Aldolase via Substrate-Binding-Guided Mutagenesis and a Stepwise Visual Screening. *ACS Catal.* 9 (5), 4462–4469.

(32) Murphy, C. D., O'Hagan, D., and Schaffrath, C. (2001) Identification of a PLP-Dependent Threonine Transaldolase: A Novel Enzyme Involved in 4-Fluorothreonine Biosynthesis in *Streptomyces Cattlea*. *Angew. Chem., Int. Ed.* 40 (23), 4479–4481.

(33) Wu, L., Tong, M. H., Raab, A., Fang, Q., Wang, S., Kyeremeh, K., Yu, Y., and Deng, H. (2020) An Unusual Metal-Bound 4-Fluorothreonine Transaldolase from *Streptomyces* Sp. MA37 Catalyses Promiscuous Transaldol Reactions. *Appl. Microbiol. Biotechnol.* 104 (9), 3885–3896.

(34) Xu, L., Wang, L. C., Xu, X. Q., and Lin, J. (2019) Characteristics of L-Threonine Transaldolase for Asymmetric Synthesis of  $\beta$ -Hydroxy- $\alpha$ -Amino Acids. *Catal. Sci. Technol.* 9 (21), 5943–5952.

(35) Heinert, D., and Martell, A. E. (1963) Pyridoxine and Pyridoxal Analogs. VII. Acid-Base Equilibria of Schiff Bases. *J. Am. Chem. Soc.* 85 (2), 188–193.

(36) Hill, M. P., Carroll, E. C., Vang, M. C., Addington, T. A., Toney, M. D., and Larsen, D. S. (2010) Light-Enhanced Catalysis by Pyridoxal Phosphate-Dependent Aspartate Aminotransferase. *J. Am. Chem. Soc.* 132 (47), 16953–16961.

(37) Kreidler, D. F., Gemmel, E. M., Schaffer, J. E., Wenciewicz, T. A., and Gulick, A. M. (2019) The Structural Basis of N-Acyl- $\alpha$ -Amino- $\beta$ -Lactone Formation Catalyzed by a Nonribosomal Peptide Synthetase. *Nat. Commun.* 10 (1), 1–13.

(38) Xu, L., Wang, L. C., Su, B. M., Xu, X. Q., and Lin, J. (2020) Multi-Enzyme Cascade for Improving  $\beta$ -Hydroxy- $\alpha$ -Amino Acids Production by Engineering L-Threonine Transaldolase and Combining Acetaldehyde Elimination System. *Bioresour. Technol.* 310, 123439.

(39) Grishin, N. V., Phillips, M. A., and Goldsmith, E. J. (1995) Modeling of the Spatial Structure of Eukaryotic Ornithine Decarboxylases. *Protein Sci.* 4 (7), 1291–1304.

(40) Eliot, A. C., and Kirsch, J. F. (2004) Pyridoxal Phosphate Enzymes: Mechanistic, Structural, and Evolutionary Considerations. *Annu. Rev. Biochem.* 73 (1), 383–415.

(41) Fairman, J. W., Jensen, M. M., Sullivan, A. H., Edwards, T. E., and Lorimer, D. PDBID: 4OT8 - X-Ray Crystal Structure of Serine Hydroxymethyl Transferase from *Burkholderia Cenocepacia* Bound to PLP and Serine.

(42) Buller, A. R., Brinkmann-Chen, S., Romney, D. K., Herger, M., Murciano-Calles, J., and Arnold, F. H. (2015) Directed Evolution of the Tryptophan Synthase  $\beta$ -Subunit for Stand-Alone Function Recapitulates Allosteric Activation. *Proc. Natl. Acad. Sci. U. S. A.* 112 (47), 14599–14604.

(43) Argiriadi, M. A., Banach, D., Radziejewska, E., Marchie, S., DiMauro, J., Dinges, J., Dominguez, E., Hutchins, C., Judge, R. A., Queeney, K., Wallace, G., and Harris, C. M. (2016) Creation of a S1P Lyase Bacterial Surrogate for Structure-Based Drug Design. *Bioorg. Med. Chem. Lett.* 26 (9), 2293–2296.

(44) Tan, K., Bigelow, L., Bearden, J., Phillips, G. N., Jr., and Joachmiak, A. PDBID SUID -The Crystal Structure of an Amino-transferase TlmJ from *Streptoalloteichus*.

(45) Raj, I., Mazumder, M., and Gourinath, S. (2013) Molecular Basis of Ligand Recognition by OASS from *E. Histolytica*: Insights from Structural and Molecular Dynamics Simulation Studies. *Biochim. Biophys. Acta, Gen. Subj.* 1830 (10), 4573–4583.

(46) Tu, Y., Kreinbring, C. A., Hill, M., Liu, C., Petsko, G. A., McCune, C. D., Berkowitz, D. B., Liu, D., and Ringe, D. (2018) Crystal Structures of Cystathionine  $\beta$ -Synthase from *Saccharomyces Cerevisiae*: One Enzymatic Step at a Time. *Biochemistry* 57 (22), 3134–3145.

(47) Percudani, R., and Peracchi, A. (2009) The B6 Database: A Tool for the Description and Classification of Vitamin B6-Dependent Enzymatic Activities and of the Corresponding Protein Families. *BMC Bioinf.* 10 (1), 273.

(48) Angelucci, F., Morea, V., Angelaccio, S., Saccoccia, F., Contestabile, R., and Ilari, A. (2014) The Crystal Structure of

Archaeal Serine Hydroxymethyltransferase Reveals Idiosyncratic Features Likely Required to Withstand High Temperatures. *Proteins: Struct., Funct., Genet.* 82 (12), 3437–3449.

(49) Kumar, S., Rosenberg, J. M., Bouzida, D., Swendsen, R. H., and Kollman, P. A. (1992) THE Weighted Histogram Analysis Method for Free-Energy Calculations on Biomolecules. I. The Method. *J. Comput. Chem.* 13 (8), 1011–1021.

(50) Toney, M. D. (2005) Reaction Specificity in Pyridoxal Phosphate Enzymes. *Arch. Biochem. Biophys.* 433 (1), 279–287.

(51) Buller, A. R., Van Roye, P., Cahn, J. K. B., Scheele, R. A., Herger, M., and Arnold, F. H. (2018) Directed Evolution Mimics Allosteric Activation by Stepwise Tuning of the Conformational Ensemble. *J. Am. Chem. Soc.* 140 (23), 7256–7266.

(52) Milić, D., Demidkina, T. V., Faleev, N. G., Phillips, R. S., Matković-Čalogović, D., and Antson, A. A. (2011) Crystallographic Snapshots of Tyrosine Phenol-Lyase Show That Substrate Strain Plays a Role in C-C Bond Cleavage. *J. Am. Chem. Soc.* 133 (41), 16468–16476.

(53) Masuo, S., Tsuda, Y., Namai, T., Minakawa, H., Shigemoto, R., and Takaya, N. (2020) Enzymatic Cascade in *Pseudomonas* That Produces Pyrazine from  $\alpha$ -Amino Acids. *ChemBioChem* 21 (3), 353–359.

(54) di Salvo, M. L., Remesh, S. G., Vivoli, M., Ghatge, M. S., Paiardini, A., D'Aguzzo, S., Safo, M. K., and Contestabile, R. (2014) On the Catalytic Mechanism and Stereospecificity of *Escherichia Coli* L-Threonine Aldolase. *FEBS J.* 281 (1), 129–145.

(55) Lane, A. N., and Kirschner, K. (1983) The Mechanism of Binding of L-Serine to Tryptophan Synthase from *Escherichia Coli*. *Eur. J. Biochem.* 129 (3), 561–570.

(56) Hale, K. J., Manaviyar, S., and Delisser, V. M. (1994) A Practical New Asymmetric Synthesis of (2S,3S)- and (2R,3R)-3-Hydroxyleucine. *Tetrahedron* 50 (30), 9181–9188.

(57) Makino, K., Okamoto, N., Hara, O., and Hamada, Y. (2001) Efficient Enantioselective Synthesis of (2R,3R)- and (2S,3S)-3-Hydroxyleucines and Their Diastereomers through Dynamic Kinetic Resolution. *Tetrahedron: Asymmetry* 12 (12), 1757–1762.